DOI: 10.13009/EUCASS2017-92

Validation and further development of 2.5D approach to description of flows in engine ducts

Vladimir Vlasenko and Vadim Talyzin**
** Central Aerohydrodynamic Institute named after Prof. N.E. Zhukovsky (TsAGI)*
1 Zhukovsky street, Zhukovsky, Moscow Region, Russia, 140180

Abstract

In 2015, 2.5D approximation for numerical simulation of flows in engine ducts was proposed. It allows two-dimensional calculations of flows in ducts with arbitrary form of cross-sections. Results of experimental validation of 2.5D approach are presented. Experimental data on model combustor with elliptic cross-sections are used. This combustor was designed within international project HEXAFLY-INT and was studied at T-131 wind tunnel of TsAGI. Comparison of 2.5D calculations with experiment for a wide range of flow regimes is given. Regimes with several stationary solutions and with flame oscillations are discussed. An idea of the 2.5D approach improvement is described.

Nomenclature

E	=	total energy per unit mass of gas
$\vec{F}_i$	=	flux of $\vec{u}$ in x_i spatial direction
i, j, k	=	spatial indices
$J_i(a)$	=	summary (molecular and turbulent) diffusive flux of parameter a in x_i spatial direction
k	=	mean kinetic energy of turbulence; as index - number of turbulence parameter
m	=	index denoting the number of gas mixture component
M	=	Mach number
n	=	coordinate in direction of unit vector of local outer normal to the duct wall
N_{sp}	=	quantity of gas mixture components
N_{turb}	=	quantity of differential equations in turbulence model
p	=	static pressure
P_t	=	total pressure
p_k^t	=	k-th parameter of turbulence model
q_i	=	summary (molecular and turbulent) diffusive flux of heat in x_i spatial direction
$S(a)$	=	source term of parameter a
t	=	time
T	=	static temperature
u_i	=	velocity components ($u_1 = u,\ u_2 = v,\ u_3 = w$)
$\vec{u}$	=	vector of conservative variables
W	=	subscript corresponding to parameters at no-slip wall
$\vec{W}$	=	vector of source terms
x_i	=	Cartesian coordinates ($x_1 = x,\ x_2 = y,\ x_3 = z$)
Y_m	=	mass fraction of m component of gas mixture
ε	=	mean rate of k dissipation
φ	=	equivalence ratio (ER)
μ	=	molecular viscosity
ρ	=	density
τ_{ji}	=	summary (molecular and turbulent) diffusive flux of ρu_j in x_i spatial direction
∞	=	subscript corresponding to free stream parameters

DOI: 10.13009/EUCASS2017-92

1. Introduction

In the previous paper [1], a new approach was proposed for approximate analysis of flow structure in the ducts of aircraft engines, especially in combustion chambers. Calculation of such flows on the basis of full 3D RANS equations for multi-component gas with finite-rate reactions, closed by differential turbulence model and by model of chemistry, requires huge volume of computer memory and huge CPU time even in the case of parallel computing. Moreover, modern physical models of chemical kinetics, turbulence and turbulence-chemistry interaction are still either insufficiently accurate or require enormous computational resources. As a result, 3D calculations provide important information about details of flow structure but cannot give accurate predictions of global characteristics of flow. Comparison of 3D calculations of flows in high-speed combustors, performed within last 15 years (e.g. [2-5]), shows that there is no progress in predictions of load distributions along duct walls, and the same accuracy of prediction may be obtained in 2D calculations. 2.5D approximation provides the possibility of multiple parametric computations of flows in ducts of rather arbitrary form at the stage of preliminary design. It gives much more information about flow structure than simple quasi-1D calculations, which are often used at this stage.
This work presents the results of experimental validation of 2.5D approach. For this purpose, experimental data on model combustor of high-speed civil aircraft was used. This combustor was designed within international project HEXAFLY-INT (7th Framework Program, Contract No. ACP3-GA-2014-620327) [6,7] and was studied at T-131 wind tunnel of TsAGI. Its duct has elliptic cross-sections. The fuel (hydrogen) is injected from two zones. In the first zone, two semi-struts generate jets of fuel directed vertically, normal to the stream; in the second zone, one central full-strut produces jets in direction of flow. Desire to perform approximate calculations of such flow in 2D formulation resulted in creation of 2.5D method [1]. Experiments were performed for a wide range of flow regimes, corresponding to cruise flight with Mach number M=6...8. Comparison of numerical simulation of these regimes in 2.5D formulation with experimental data has allowed to validate the 2.5D technology.

2. Brief description of 2.5D approach

In 2.5D approximation, the real 3D flow in a duct is replaced by a flow with parameters that are constant along coordinate axis x_3. It may be treated as a result of 3D flow averaging along x_3 axis. Calculation is performed in (x_1; x_2) plane, but variable width of duct in x_3-direction is taken into account.
3D RANS equation system can be represented as follows:

$$\frac{\partial \vec{u}}{\partial t}+\frac{\partial \vec{F}_1}{\partial x_1}+\frac{\partial \vec{F}_2}{\partial x_2}+\frac{\partial \vec{F}_3}{\partial x_3}=\vec{W}\,.$$

Derivation of equations for 2.5D analogue of 3D flow is given in [1]. These equations have the following structure:

$$\frac{\partial}{\partial t}\left(\vec{u}h_3\right)+\frac{\partial}{\partial x_1}\left(\vec{F}_1h_3\right)+\frac{\partial}{\partial x_2}\left(\vec{F}_2h_3\right)+\left(\vec{F}_1^{-}\frac{\partial x_3^{\min}}{\partial x_1}-\vec{F}_1^{+}\frac{\partial x_3^{\max}}{\partial x_1}+\vec{F}_2^{-}\frac{\partial x_3^{\min}}{\partial x_2}-\vec{F}_2^{+}\frac{\partial x_3^{\max}}{\partial x_2}+\vec{F}_3^{+}-\vec{F}_3^{-}\right)=\vec{W}h_3\,. \qquad \textbf{(1)}$$

Here $x_3^{\min}(x_1,x_2)$ and $x_3^{\max}(x_1,x_2)$ are x_3-coordinates of the duct walls, $h_3(x_1,x_2)=x_3^{\max}(x_1,x_2)-x_3^{\min}(x_1,x_2)$, $\vec{F}_i^{+}$ is the value of flux vector at the duct wall with coordinate $x_3^{\max}$, $\vec{F}_i^{-}$ is the flux value at the duct wall with coordinate $x_3^{\min}$. Vectors $\vec{u}$, $\vec{F}_i$ and $\vec{W}$ have the following structure:

$$\vec{u}=\begin{bmatrix}\rho\\ \rho u_j\\ \rho E\\ \rho p_k^t\\ \rho Y_m\end{bmatrix},\quad \vec{F}_i=\begin{bmatrix}\rho u_i\\ \rho u_j u_i+p\delta_{ij}+\tau_{ji}\\ \rho E u_i+pu_i+\tau_{ji}u_j+q_i+J_i(k)\\ \rho p_k^t u_i+J_i(p_k^t)\\ \rho Y_m u_i+J_i(Y_m)\end{bmatrix},\quad \vec{W}=\begin{bmatrix}0\\0\\0\\S(p_k^t)\\S(Y_m)\end{bmatrix}. \qquad \textbf{(2)}$$

DOI: 10.13009/EUCASS2017-92

In Eq. (2), the spatial indices i and j may take values 1 and 2 (1 corresponds to x_1 axis, 2 – to x_2 axis), $k = 1,..., N_{turb}$, $m = 1,..., N_{sp} - 1$. Summation over repeated spatial indices is implied.

Fluxes through the duct walls in Eq. (1), $\vec{F}_i^+$ and $\vec{F}_i^-$ ($i = 1,2,3$; $i = 3$ corresponds to x_3 axis), are calculated using special procedure. In determination of wall fluxes, the model of 3D flow is used that assumes the flow to be consisted of inviscid core, where the pressure is constant along x_3 direction, and of boundary layers, where the flow is decelerated to zero velocity. Due to the fact that the pressure is practically constant across boundary layer, the wall pressure is taken to be equal to $p(x_1, x_2)$ - pressure in 2.5D analogue of this 3D flow. Molecular diffusive fluxes of momentum, heat and turbulence parameters in the direction of the normal to wall are determined by local structure of boundary layer. In 2.5D calculation, boundary layers arise only near the duct boundaries with coordinates $x_2 = x_2^{\max}$ and $x_2 = x_2^{\min}$. Molecular fluxes through the duct side walls (they have form $\mu_W \frac{\partial f}{\partial n}$) are estimated through linear interpolation in x_2 between $x_2^{\min}$ and $x_2^{\max}$. At that, it is assumed that direction of fluxes coincides with local direction of normal to the duct side wall. Details may be found in [1].

It is worth to note that averaging of flow along the third coordinate was previously used for reduction of 3D equations to 2D equations by A.N.Kraiko with co-authors [8], but only for Euler equations and for narrow duct.

3. Experiments in T-131 wind tunnel

At present time in many countries various concepts of high-speed vehicles for civil passenger transportation are developed for long distances with travel times much less than could be attained on the existing civil aircraft. In framework of the European project LAPCAT-II [9], several high-speed passenger vehicle concepts were studied on the basis of hydrogen fuelled air breathing engines. Aim of this work was to assess the technical feasibility of a high-speed vehicle for civil transportation that could fly to diametrically opposite points (e.g. from Brussels to Sydney) at cruise speeds ranging from Mach number M= 5 to 8. The claimed performances were verified on the basis of simulations and on-ground experiments. The next step is the verification by flight experiment which is one of the main goals of the international coordinated project HEXAFLY-INT.

Two concepts of the Experimental Flight Test Vehicle (EFTV) were proposed for study. A first concept is a glider vehicle, i.e. without any on-board propulsion. A second concept is a powered concept, i.e. with scramjet propulsion system. The first concept will evolve into in flight experiment while the second concept is studied numerically and experimentally on-ground by Russian entities such as TsAGI, CIAM, FRI and MIPT. Configuration of the EFTV powered concept having a length of L≈3 m developed by European partners [10,11] is shown on the Figure 1.

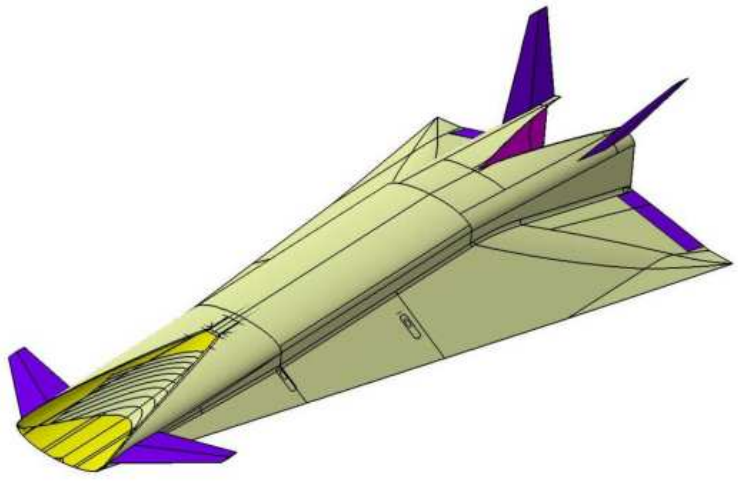

Figure 1: Powered concept under study

At T-131 wind tunnel of TsAGI, model of EFTV power plant was tested on the connected-pipe facility. The model consisted of seven sections (see Figure 2). First three sections together constituted the connecting pipe, placed in tests between the fire heater and the model of EFTV inner duct. Section 1 is transitional insert between the heater and the nozzle; section 2 is short interchangeable part with round critical section of different area, with system of water cooling; section 3 is expanding part of supersonic nozzle with transition from round section to ellipse.

DOI: 10.13009/EUCASS2017-92

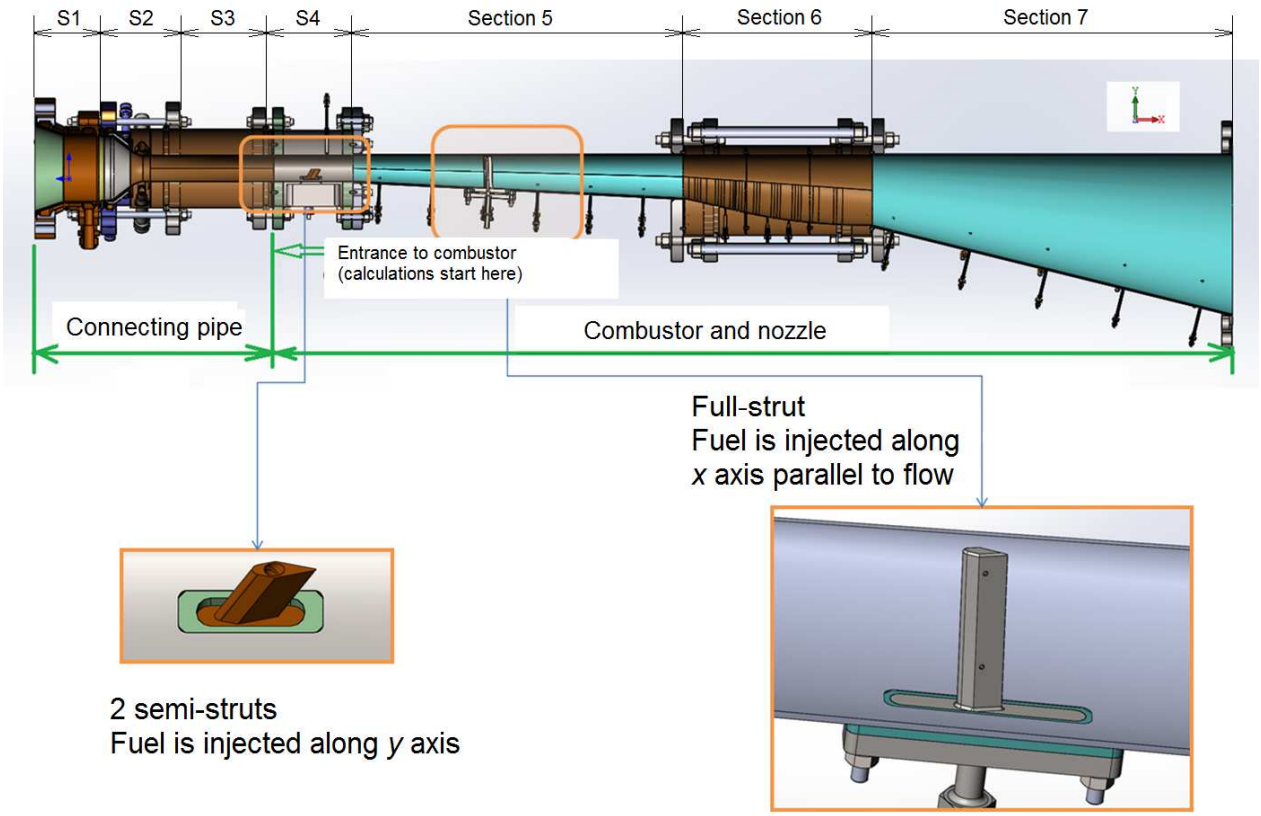

Figure 2: Model of HEXAFLY-INT power plant duct (lateral view) and geometry of struts for fuel injection

The rest 4 sections (Fig.2) reproduce the elements of EFTV duct. Sections 4 and 5 have elliptical cross sections. Section 4 contains the first injection section, where two short arrow-like semi-struts, inclinated by 60° to longitudinal axis, are mounted at the lower wall. Leading edges of semi-struts has radius 2 mm, trailing edge - 0.3 мм. Hydrogen is injected in vertical direction through the injection hole with diameter 5 mm, that is placed at the end face of semi-strut. Injectors are profiled to create fuel jets with Mach number $M = 2$. Section 5 is the main part of combustor. It contains the main full-strut, mounted in longitudinal symmetry plane. The full-strut is placed nearly vertically and contains two pairs of injection holes at both sides. The radius of injection holes is 1.4 mm. The full-strut also has arrow-like form with radii of edges 2 mm (leading edge) and 0.2 mm (trailing edge). Section 6 is expanding insert with transition of cross-section from ellipse to circle, and the section 7 (so-called "2D" nozzle) is expanding supersonic nozzle with round sections.

4. Organization of calculations and typical flow structure

Preliminary 3D calculation with hydrogen injection, but with frozen chemical reactions has shown that variation of flow parameters along y axis is less significant than along z axis. Consequently, 2.5D calculations in $(x; y)$ plane would give picture of fuel-air mixing that would differ principally from 3D calculations. So, it was decided to perform 2.5D calculations of the combustion chamber in (x, z) plane [1].

Unsteady Reynolds equations system in approximation of 2.5D flow (1)-(2) is solved. For the description of turbulence, $q-\omega$ model [12] is used. It is original version of T.J.Coakley's turbulence model with blending function similar to one used in F.R.Menter's SST model. Therefore, the parameter N_{turb} was equal to 2, and two additional differential equations were solved for $p_1^t = q \equiv \sqrt{k}$ and for $p_2^t = \omega \equiv \varepsilon / k$. Though the hydrogen is used as a fuel, the inflow at EFTV duct entrance contains products of kerosene combustion in fire heater. So, for the description of chemical reactions the simplified kinetic mechanism, containing reactions between $N_{sp} = 9$ components (H, O, OH, H_2O, O_2, H_2, CO, CO_2 with inert nitrogen N_2) [13], is used. Turbulence-combustion interaction is neglected. The duct walls are considered as heat-insulated; to avoid extreme compression of grid near the walls, an original boundary condition of the class "wall functions" (see [12]) was used.

DOI: 10.13009/EUCASS2017-92

Mathematical model of geometry and computational grid are shown in Fig.3. Computational domain is a projection of the EFTV duct sections 4-7 (see Fig. 2) on (x, z) plane, with addition of expanding buffer block with coarse grid. The mathematical model contains the section of central full-strut; short semi-struts, injecting the fuel along y axis, are not reproduced explicitly. Computational grid consists of 28 blocks and contains 117248 cells totally; it is compressed around the central full-strut. Injection of hydrogen is simulated by adding of sources of mass, momentum, energy, turbulence and mass of fuel in the locations, where the hydrogen injectors are placed in real experimental model (Fig. 2).

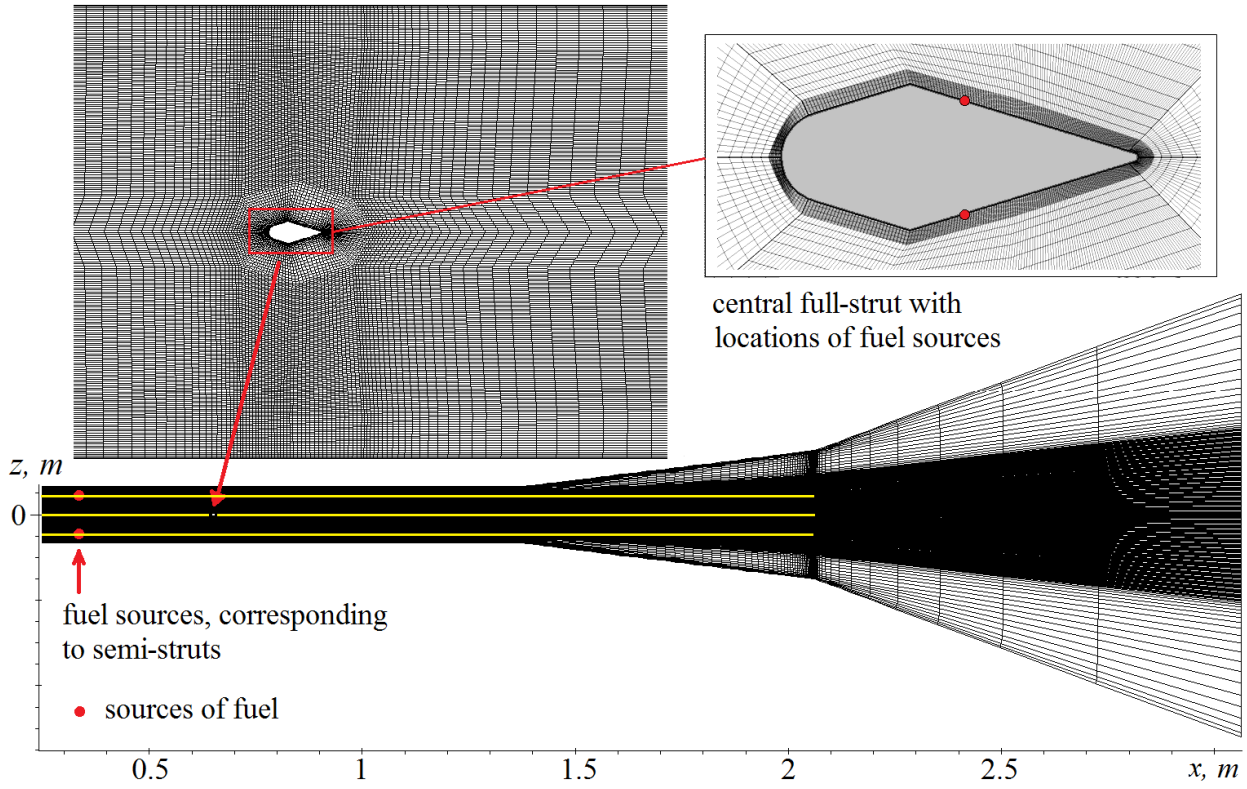

Figure 3: Grid for 2.5D computations in (*x*,*z*) plane and locations of hydrogen sources.
Yellow lines – sections of pressure mesurements in experiments

Numerical method of the 2nd approximation order in all variables is used. This method includes explicit monotonic Godunov-Kolgan-Rodionov scheme [14,15] for convective fluxes, explicit modified central-difference approximation [15] of diffusive terms and local implicit approximation [16] of source terms. Multi-block regular grids are used in calculations. To accelerate convergency to stationary solution, local time stepping [15] is ised. If unsteady process should be described correctly, then computation is accelerated with the use of fractional time stepping [15].

In Fig.4 the typical flow structure in model combustor is demonstrated. It corresponds to flight Mach number $M_\infty = 7$ and integral equivalence ratio $\varphi \approx 0.935$. Injection scheme is 43.4%-43.4%-13.2% (it means than 43/4% of total mass-flow rate of hydrogen is injected from each of two semi-struts and the rest 13.2% - from the central full-strut). In this regime, average Mach number at the entrance in the inviscid core is close to 2.7. To demonstrate details, only part of the duct is shown, and the scale along the duct width is increased. This field shows that oblique shock waves arise ahead of the fuel jets, injected from the semi-struts. In the place of their interaction with wall, small separation of boundary layer arises. Field of temperature shows that in the supersonic jets from semi-struts a weak heat release proceeds initially only on the surfaces of the jets (because of low temperature of injected hydrogen – 163 K).

More intensive shock wave is formed ahead the blunted leading edge of the central full-strut. Its interaction with boundary layers on the duct walls leads to formation of separation zones of higher size. Oblique shocks, produced by these separations, intersect with leading shock wave from central full-strut in the region of passage of jets from two semi-struts, with lower Mach number. As a result, these shocks intersect irregularly, with formation of Mach disks, curved due to the flow inhomogeneity in the hydrogen jets. Behind the Mach disks, there are regions of subsonic flow. Growth of pressure and of temperature in shock-wave structures accelerates the reaction, and decrease of

DOI: 10.13009/EUCASS2017-92

velocity in this region lead to longer residence of fuel in the reaction zone. Downstream from the central full-strut, combustion proceeds in regions of subsonic or transonic flow. Curved leading shock wave ahead of the central pylon and curved Mach disks, and also boundary layer separations generate vorticity and become strong generators of turbulence. Growth of turbulence helps to combustion downstream from the central full-strut through the transport of heat from combustion zones to cold flow regions and through the transport of reagents to combustion zones. In the separations on the walls there is no combustion because of the absence of fuel. Combustion practically stops at considerable distance upstream from the section, where the duct width begins to grow. This effect is mainly due to the fact that here the duct area starts to grow (the width of the duct is still constant, but its height starts to increase along *x* axis). Stopping of the heat release and growth of the duct area lead to growth of the Mach number.

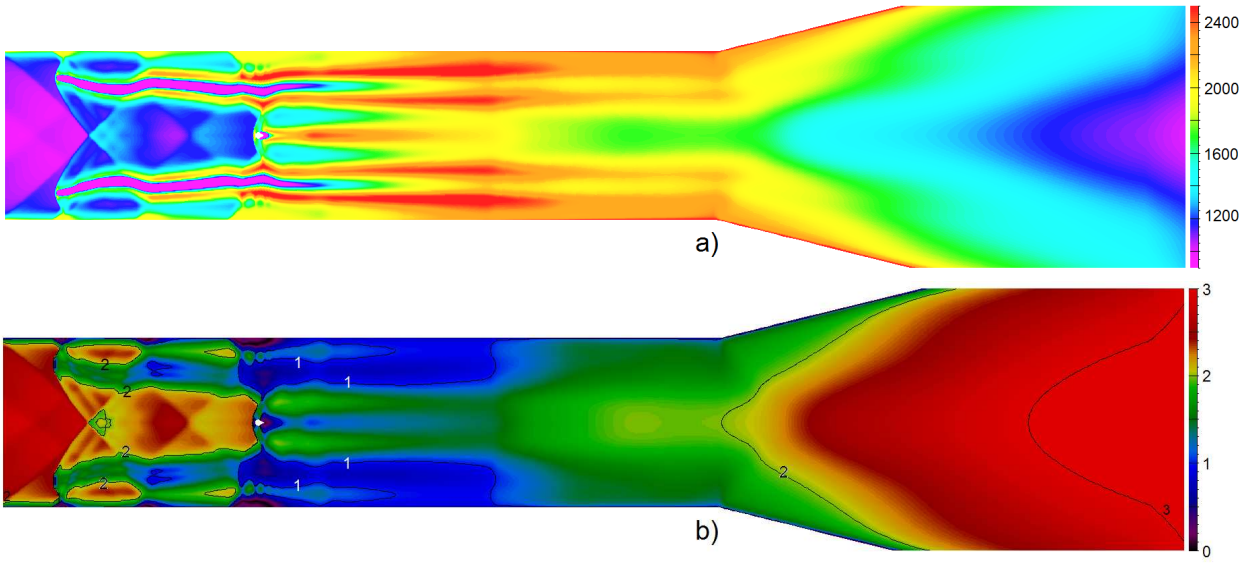

Figure 4: Typical flow structure: a) field of static temperature [K]; b) field and isolines of Mach number

5. Comparison of 2.5D calculations with experiment

After experiments in T-131B wind tunnel of TsAGI, validation of the used numerical technology was performed. For this purpose, experimental runs were simulated in calculations. Calculated pressure distributions along the chamber walls were compared with experiments.

$M_\infty = 7$, $M_\infty = 7.4$ and $M_\infty = 6$. At the flight regime $M_\infty = 7$, the flow parameters at EFTV entrance are $M \approx 2.6$, $P_t \approx 14$ atm, air mass-flow $G \approx 1.55$ kg/sec. At the flight regime $M_\infty = 7.4$, inflow parameters are $M \approx 3$, $P_t \approx 12$ atm, $G \approx 0.7$ kg/sec, and for the regime $M_\infty = 6$ inflow parameters are $M \approx 2.3$, $P_t \approx 10$ atm, $G \approx 1.6$ kg/sec.

In addition to inflow regime, experimental runs differed by the hydrogen mass-flow rate (i.e. by equivalence ratio φ). Central full-strut was used as injector only in part of runs. In one experimental run it was destroyed by flame, and in following runs the hydrogen mass flow rate was equidistributed between the semi-struts. In part of runs, imitator of central full-strut was mounted at its place, but hydrogen was injected only from the semi-struts.

In Fig. 5, an example of the static pressure longitudinal distributions is shown. These distributions were obtained for the same flow regime as in Fig.4. Upper picture shows the distributions along central line that is shown in Fig.3, and the lower picture shows distributions along lateral lines, which are also shown in Fig.3. Calculated data along two lateral lines coincide. Experimental data, obtained along side lines, are shown by different triangle markers. Difference between markers, corresponding to the same longitudinal coordinates, characterizes the experimental data scatter. Blue curves correspond to cold flow without fuel injection, red curves – to hot flow with hydrogen injection and combustion.

For this flow regime, 3D calculation of cold flow without fuel injection has also been performed (on comparable grid). Results of this calculation are also shown in Fig.5; they differ from 2.5D calculation data because of difference in local structure of 3D flow and *y*-averaged flow parameters, which are simulated in 2.5D flow, and also because of errors that are intrinsic to 2.5D approximation (see Section 8 of this paper). Nevertheless, discrepancy of 3D calculation data and experiment is not better than the errors of 2.5D calculation. It is characteristic for modern state-

DOI: 10.13009/EUCASS2017-92

of-the-art of high-speed combustor flow simulations. Modern models of turbulence and combustion still cannot provide adequate description of real flows. From this viewpoint, 2.5D approximation is very good way to estimate the real flow characteristics, if one takes into account that computational cost of 2.5D approach are lower by an order than computational cost of 3D calculations.

Also 2.5D computations in the (x, y) plane were performed for this regime. Upper picture in Fig.5 shows the pressure distributions along upper and lower walls of the duct (in its symmetry plane), obtained in these computations. One may see that data of calculations in the (x, y) plane are much further from the experiment than the data of calculations in (x, z) plane. Therefore, the choice of (x, z) plane for 2.5D calculations was correct.

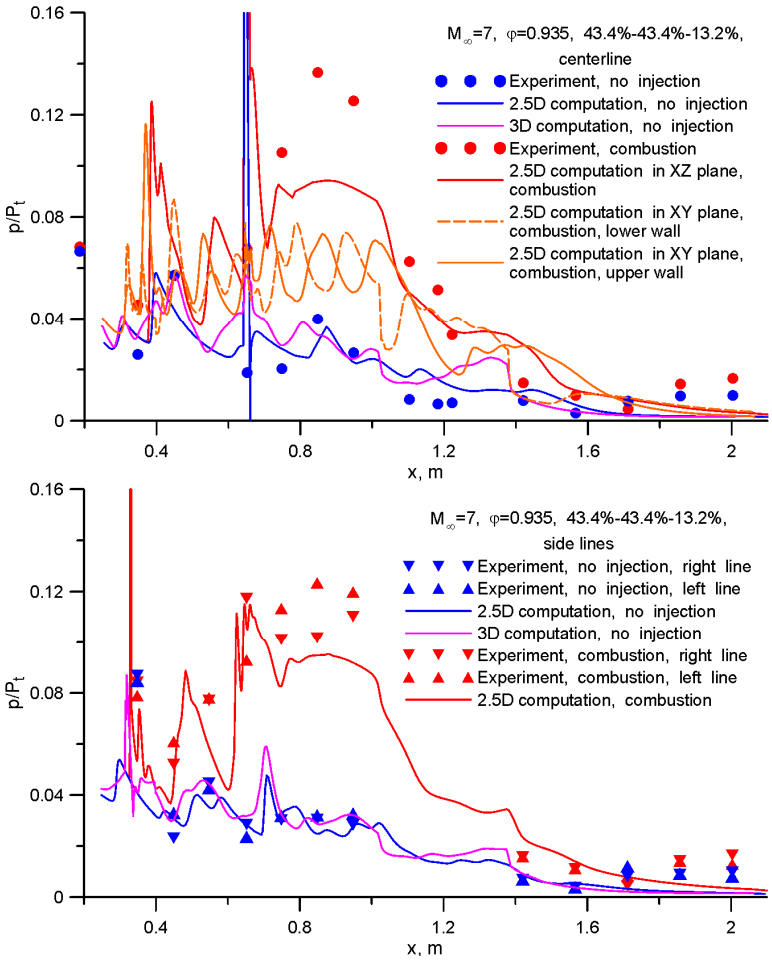

Figure 5: Longitudinal distributions of pressure for the same run as in Fig.4 (M_∞ = 7, φ=0.935)

With the exception of the interval $0.85 < x < 1.0$ m at the duct centerline, the discrepancy between 2.5D calculation in (x, z) plane and the experiment is close to experimental data scatter. It is also necessary to take into account that the experimental data are local, whereas data of 2.5D calculations are averaged along vertical lines passing through the current point of (x, z) plane. Averaging should smooth the peaks in pressure distribution, and one may see this effect in Fig.5.

For all considered regimes, the same quality of agreement between 2.5D calculations and the experiment is obtained. Figure 6,a,b demonstrates another examples, obtained for M_∞ = 7.4, and Figure 6,c,d – for M_∞ = 6. These pictures have the same specific features as in Fig.5. It is especially important that very different flow regimes were considered in calculations– from intensive combustion in Fig.5 and in Fig.6,c,d to practically cold flow in Fig.6,a. In all cases. 2.5D calculations reproduce correctly the qualitative features of pressure distributions.

DOI: 10.13009/EUCASS2017-92

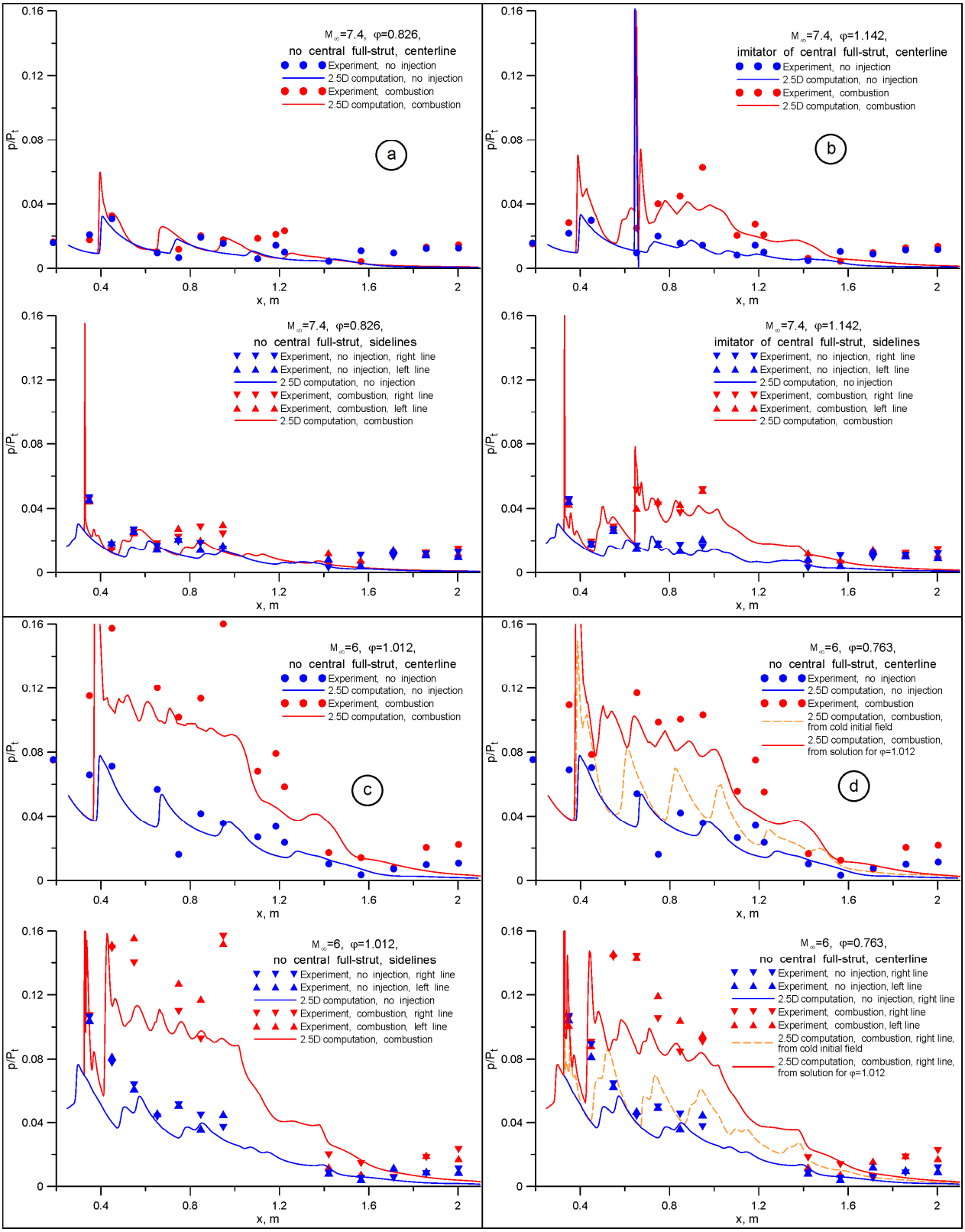

Figure 6: Longitudinal distributions of pressure for the experimental runs, corresponding to M_∞ = 7.4 (a - φ=0.826, b - φ=1.142) and to M_∞ = 6 (c - φ=1.012, d - φ=0.763)

DOI: 10.13009/EUCASS2017-92

6. Regimes with multiple stationary solutions

In simulation of flow regimes, corresponding to the flight Mach number $M_\infty = 6$, 2.5D calculations did not immediately yield positive results. For some regimes the combustion practically did not developed in calculation (see orange curves in the plots for the regime $\varphi = 0.763$ – Fig.6,d and the field of temperature in Fig.7,b). But in the experiment intensive combustion was observed. It means that in real 3D flow picture the sufficient-for-combustion conditions arise locally, but in *y*-averaged field of 2.5D flow the conditions are not sufficient for the flame ignition.
In those regimes the mixture was too lean for self-ignition. But in the regime $\varphi = 1.01$ the mixture was close to stoichiometry, the self-igntion took place, and intensive combustion appeared – see Figures 6,c and 7,a. Pressure distributions, qualitatively similar to experimental data, were obtained. After that an attempt to start calculation for the regime $\varphi = 0.763$ from the converged field for the regime $\varphi = 1.01$. It allowed to get stationary solution with developed combustion and to obtain pressure distributions that were much more close to experimental data (see red lines in Fig.6,d and temperature field in Fig. 7,c).

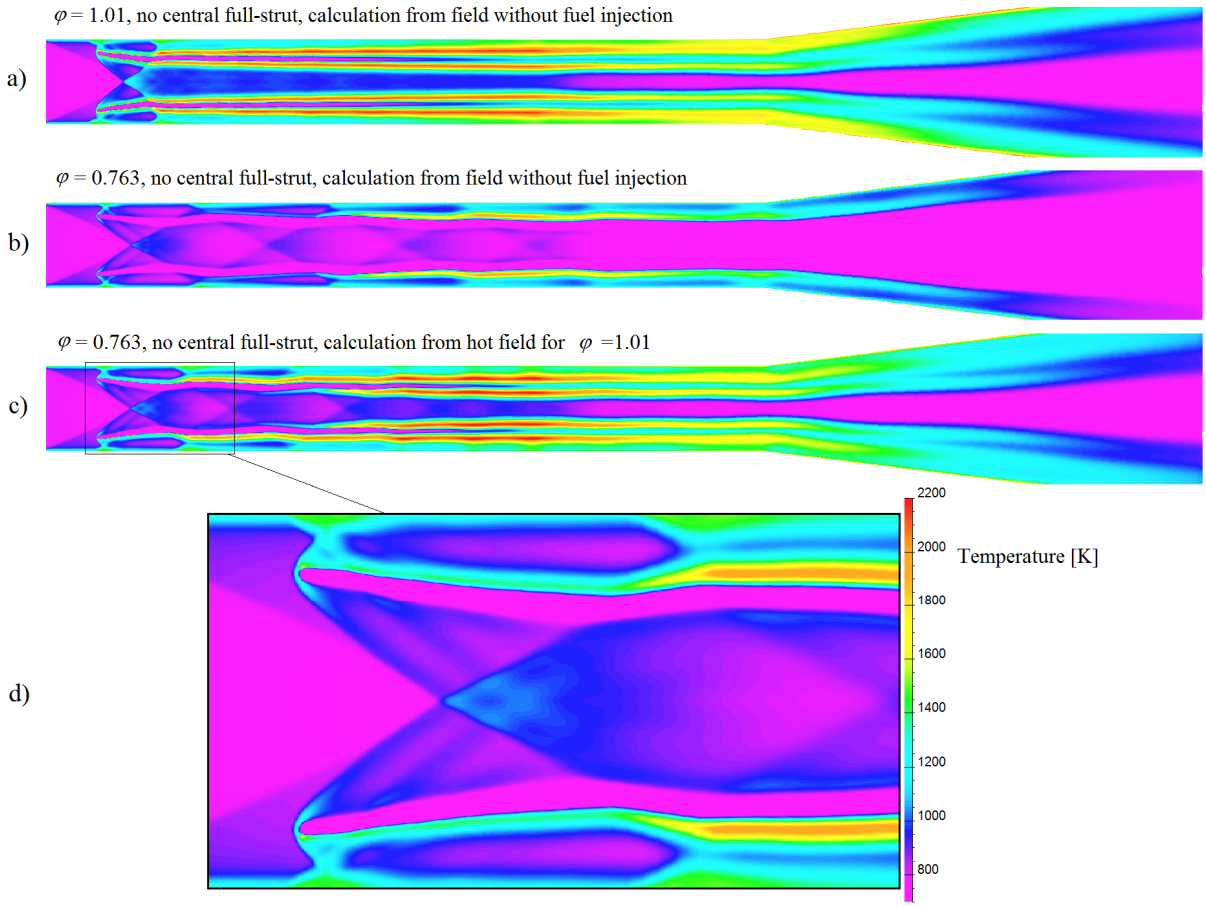

Figure 7: Fields of temperature for $M_\infty = 6$ in calculations of experimental runs without central full-strut: a - $\varphi = 1.01$; b,c,d – converged fields for $\varphi = 0.763$, obtained from different initial fields

Hysteresis phenomena (dependence of the stationary state upon pre-history) are characteristic to flows with combustion. The most well-know example is solution of task about well-stirred reactor [17-18].
Analysis of the obtained flowfield shows that in the case of calculation start from hot field the small region with low velocity, high temperature and high pressure is kept past the shock wave in the vicinity of the hydrogen jet flowing from the semi-strut (see Fig.7,d). After passage of fresh combustible mixture through this zone, reactions start in the mixture and prepare it to self-ignition that take place after passage through the second oblique shock wave, produced by another semi-strut. It is possible that somewhat another but qualitatively similar mechanism of self-ignition is realized in reality. Most probably, the stagnation region in the semi-strut wake plays the role of the flame stabilizing reactor.

DOI: 10.13009/EUCASS2017-92

7. Regimes with oscillations of flame

In some regimes, longitudinal oscillations of combustion zone appeared. These oscillations produced essential variation of the longitudinal force, applied to duct walls. The flame periodically propagated upstream and reached the duct entrance. It was a serious problem, because the calculations were performed with local time stepping (LTS, see [15]) to accelerate convergence to stationary state. If stationary state is not reached, then the flowfields, obtained in calculation with LTS, do not satisfy to conservation laws. Moreover, when the flame reached the duct entrance, the flow near the entrance became subsonic throughout, and the entrance boundary condition with given flow parameters began to work incorrectly, leading to violation of given mass-flow rate. So, for the regime $M_\infty = 7$, $\varphi = 1.101$ the calculation with fractional time stepping (FTS, see [15]) was performed. The FTS technology allows to describe unsteady processes correctly. To impose the entrance boundary condition correctly, the entrance section was moved into supersonic part of the connecting pipe. In computation, flame oscillations finally became periodic. Structure of oscillations during one period appeared to be very complex. In Fig.8 the fields of temperature T, obtained in the most characteristic time moments of calculation with FTS, are shown; Figure 9 shows the fields of longitudinal velocity u in the same time moments. In Figure 9 the isoline $u = 0$ is shown; it points to position of recirculation zones.

In the moment “a” in Figures 8-9 the state may be seen, when near the semi-struts the flow structure similar to Fig.4 is realized. Downstream one may see near the walls the combustion of hydrogen that came to walls in previous time moments. In the beginning of combustion zone at the wall there is small separation of boundary layer. The shock wave, produces by the separation, crosses the hydrogen jet from semi-strut and leads to start of heat release on the outer surface of the jet. To the next time moment (“b”) the essential quantity of heat is released in jets, leading to decrease of velocity and growth of pressure in the duct. As a result the separation zone near the wall grows in size, resulting in intensification of combustion inside the semi-strut jet and producing the duct throttling. Shock wave before the heat release starts the reverse motion upstream (to the left – see the moment “c”). Separation near the wall follows this shock wave and after some time joins with primary separation at the wall (that is produced by oblique shock wave from the semi-strut) - moment “d”. Due to upthrust by the heat release, this separation grows and finally involves the semi-strut hydrogen jet. The jet turns towards the wall (moment “e”). Fresh cold hydrogen flows inside the recirculating zone of separation, resulting in abrupt increase of its size. The separation shifts from the duct into the connecting pipe (moment “f”). At that, the separation appears to be filled with hydrogen, and because of absence of oxidizer the combustion is stopped there, with the exception of mixing layer at the outer boundary of separation. As a result, the size of separation zone decreases. Downstream from semi-struts, new separations also arise on the walls. In the moment “g” the leading separation zone stops to interact with the semi-strut. Combustion in the leading separation ends quickly, its size continues to decrease, and this separation is shifted downstream. The semi-strut jet turns to right, directing the cold hydrogen into separation zones at the wall (moment “h”). Finally, the leading separation returns to its initial position in the place, where the oblique shock from semi-strut intersects with the wall. To the right from this place the regions of slowly rotating flow, filled by cold fuel, are carried downstream (moment “i”). Flow structure returns slowly to initial state (moment “j”). After that the process repeats.

In Figure 10, instant distributions of pressure along the centerline and along side lines are shown in two moments of unsteady calculation. Also the distribution, averaged over the period, is plotted. Scatter between these curves is close to the experimental data scatter, and agreement of calculation with experiment is good almost everywhere.

Also the calculation of this flow with local time stepping (LTS) was performed. Because of incorrect description of unsteady processes, structure of oscillations in calculations with LTS differs essentially from oscillations in calculation with FTS. However, if one averages unsteady flow, obtained with LTS, then the averaged flowfield and the averaged pressure distributions appear to be close to averaged results of the calculation with FTS – see orange curves in Fig.10. Therefore, if one has no time for the prolonged calculation with FTS, it may be recommended (as palliative) to perform calculation with LTS up to periodical state with following averaging. But in this case the correctness of the obtained solution cannot be guaranteed.

DOI: 10.13009/EUCASS2017-92

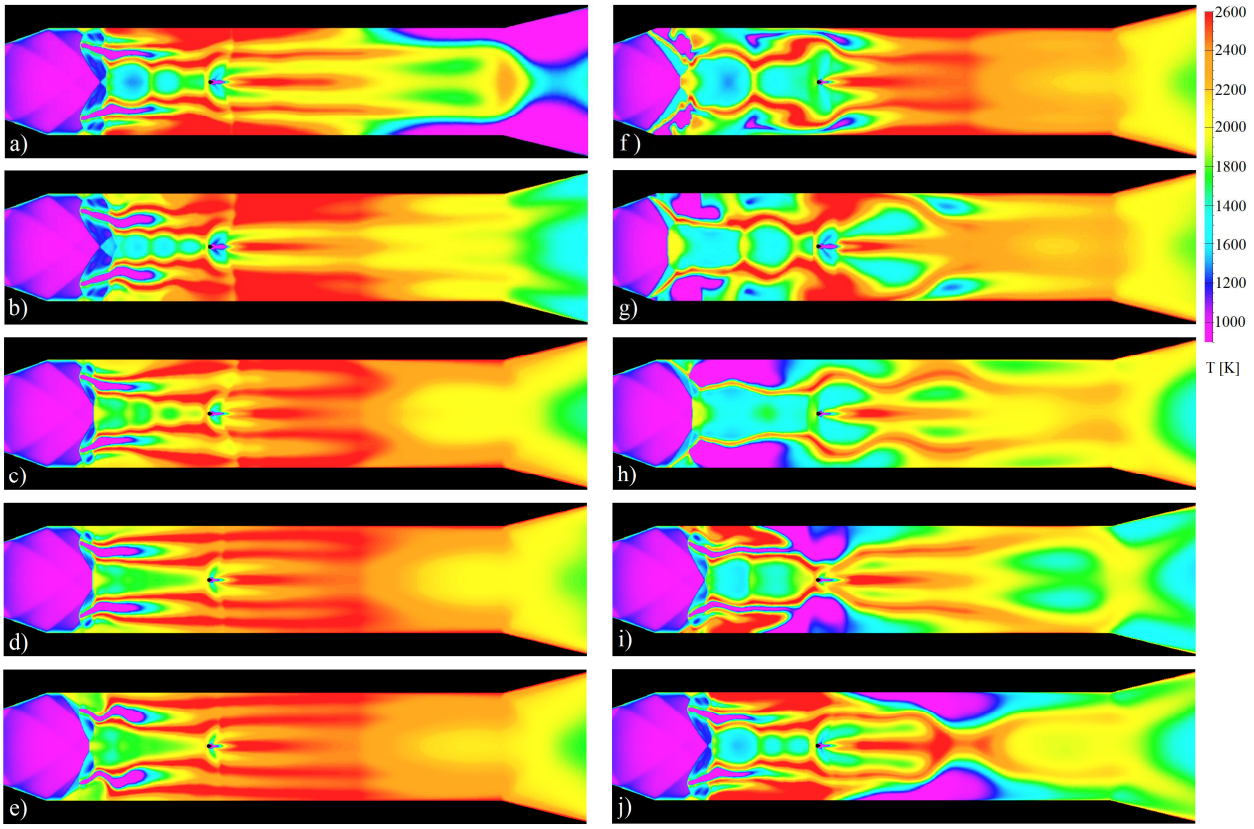

Figure 8: Sequential fields of temperature T in calculation for the regime $M_\infty = 7$, $\varphi = 1.101$

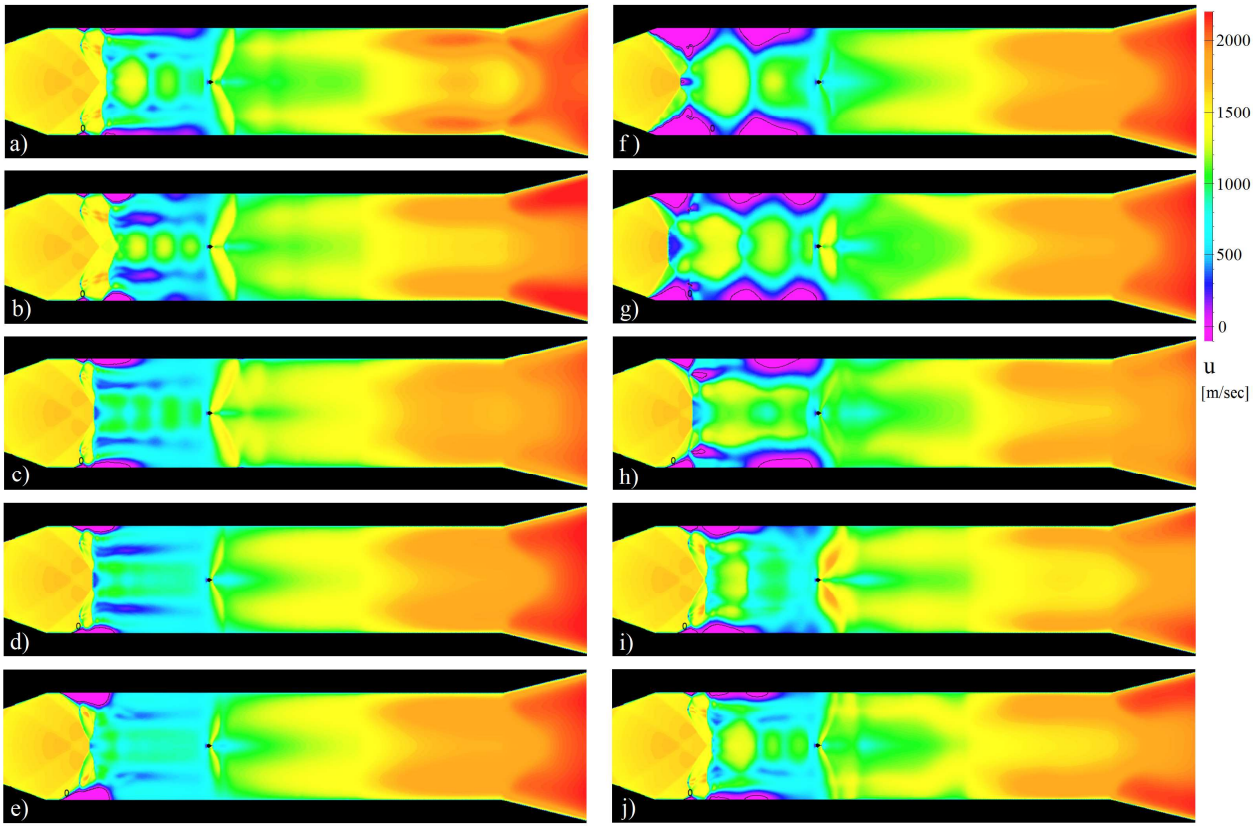

Figure 9: Sequential fields of longitudinal velocity u in calculation for the regime $M_\infty = 7$, $\varphi = 1.101$

DOI: 10.13009/EUCASS2017-92

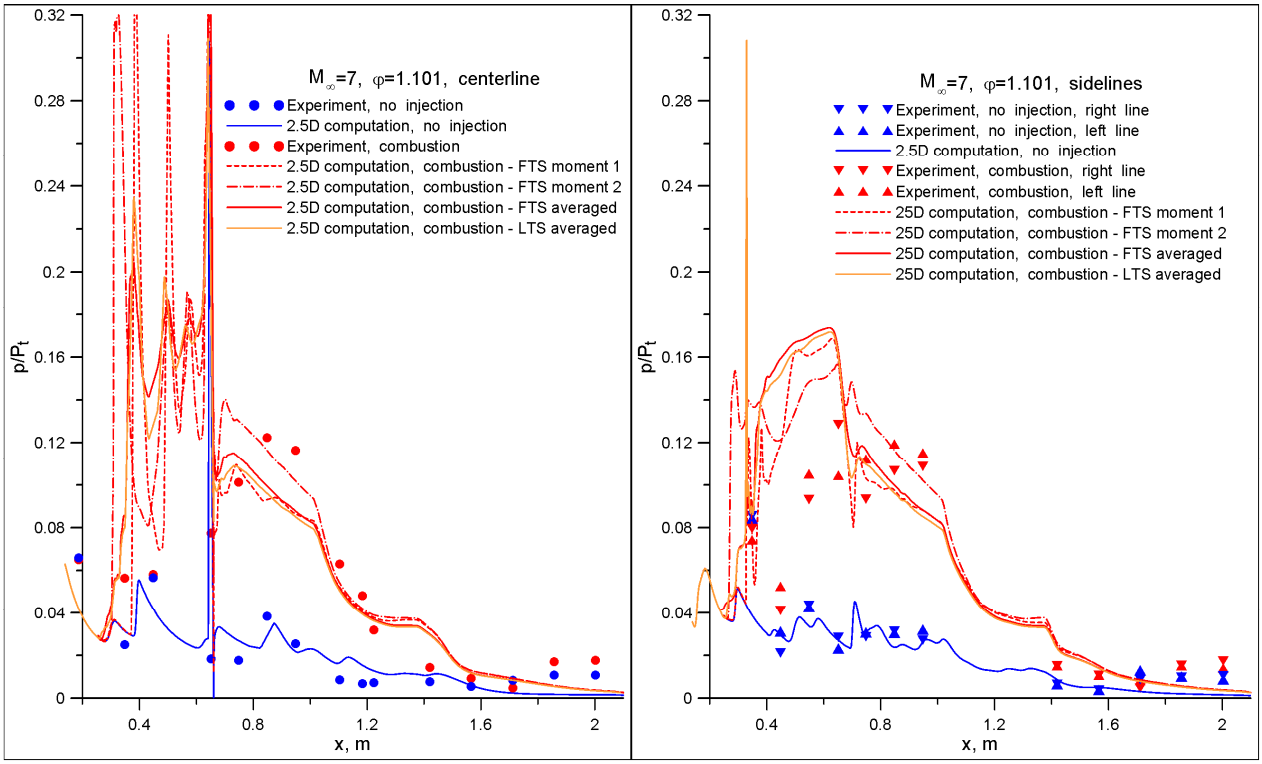

Figure 10: Longitudinal pressure distributions for the experimental run, corresponding to Fig.8-9 (M_∞ = 7, φ=1.101)

8. Possible way to improve accuracy of 2.5D calculations

Fluxes and source terms in equations (1) are calculated using the same formulas as corresponding terms in the initial equation system of 3D flow. But parameters of 2.5D flow (in fact, z-averaged parameters of real flow) are substituted into these formulas. Naturally, this approach to description of 3D flow is approximate, because it is assumed that z-averaged fluxes and sources in equation of gas motion can be calculated by usual formulas, where z-averaged gas parameters are substituted. Average of nonlinear function does not coincide with value of this function after substitution of average values of its arguments. Therefore, fluxes and source terms are determined with some errors. It is the main reason of the 2.5D approximation inaccuracy.

It is possible to propose the following way to improve the accuracy of 2.5D calculations. 2.5D computations may be performed in (x;y) and (x;z) planes simultaneously. Profiles of flow parameters, obtained in one computation, may be considered as samples for flow averaging along x_3-axis in another computation. In each plane, coefficients $K_f = \left\langle f(\vec{U}(x_3)) \right\rangle \Big/ f\left(\left\langle \vec{U}(x_3) \right\rangle\right)$ may be determined (here f are such parameters as convective fluxes in directions x_1, x_2 and chemical source terms in RANS equations, $\vec{U}$ is the vector of conservative variables, $x_3 = z$ for computation in (x;y) plane and $x_3 = y$ for computation in (x;z) plane). After that, coefficients K_f, obtained in one computation, may be used for correction of $\left\langle f \right\rangle$ in another computation.

9. Concluding remarks

On the basis of comparison with experimental data for 19 flow regimes, the validation of new 2.5D method for calculation of flows in ducts is performed. For all regimes, satisfactory agreement of calculated pressure distributions with experiment is obtained. Therefore, 2.5D method allows to predict the most important physical features of flow and predicts loads on duct walls with engineering accuracy, that is enough for multiple parametric calculations at the stage of engine preliminary design or at the stage of experiment preparation.

DOI: 10.13009/EUCASS2017-92

Acknowledgement

Part of this work is performed within the 'High-Speed Experimental Fly Vehicles-International' project fostering International Cooperation on Civil High-Speed Air Transport Research. HEXAFLY-INT, coordinated by ESA-ESTEC, is supported by the EU within the 7th Framework Programme Theme 7 Transport, Contract no.: ACP0-GA-2014-620327. Further info on HEXAFLY-INT can be found on http://www.esa.int/hexafly-int. Studies of unsteady regimes on the basis of FTS method and further improvement of 2.5D approach are supported by Grant of the Ministry of Education and Science of Russian Federation (agreement No.14.G39.31.0001).

References

[1] Vlasenko, V. V., and Shiryaeva, A. A., "2.5D approximation for numerical simulation of flows in engine ducts," 6th European Conference for Aeronautics and Space Sciences (EUCASS 2015), Kraków (Poland), 29 June - 3 July, 2015, 14 pages. Full text is available for participants at http://www.eucass2015.eu/detailed-programme/. Selected for publication in *EUCASS 2015 Propulsion Physics Volume*.

[2] Rodriguez, C., & Cutler, A. 2013. CFD analysis of the SCHOLAR scramjet model. In: *12th AIAA International Space Planes and Hypersonic Systems and Technologies*. 7039.

[3] Karl S., Hannemann K., Mack A., Steelant J. 2008. CFD analysis of the HyShot II scramjet experiments in the HEG shock tunnel. In.: *15th AIAA International Space Planes and Hypersonic Systems and Technologies Conference*. 2548.

[4] Yentsch R.J., Gaitonde D.V. 2014. Numerical Investigation of Dual-Mode Operation in a Rectangular Scramjet Flowpath. *Journal of Propulsion and Power*, Vol.30, No.2: 474-489.

[5] Xing F., Cai J., Huang Y., Yao Y. 2017. Numerical analysis of HyShot Scramjet Model with different throat heights. In: *21st AIAA International Space Planes and Hypersonics Technologies Conference*. 2121.

[6] Pezzella, G., Carandente, V., Scigliano, R., Marini, M., & Steelant, J. (2015, March). Aerothermal Environment Methodology of the Hexafly-INT Experimental Flight Test Vehicle (EFTV). In *8th European Symposium on Aerothermodynamics for Space Vehicles*. 2-6.

[7] Pezzella, G., van Brummen, S., & Steelant, J. 2015. Assessment of Hypersonic Aerodynamic Performance of the EFTV-ESM Configuration in the Framework of Hexafly-INT Research Programme.In: *8th European Symposium on Aerothermodynamics of Space Vehicles.*

[8] Kraiko, A. N., Polyanskii, A. R., and Tillyaeva, N. I. 1992. Variational problem of optimum side wall design for a narrow three-dimensional nozzle. *Fluid dynamics*, Vol.27, No.2: 230-238.

[9] Steelant J. and Langener T. The LAPCAT-MR2 hypersonic cruiser concept. 2014. In: *29th Congress of the International Council of the Aeronautical Sciences (ICAS), St. Peterburg, September 7-12*.

[10] Langener T., Steelant J., Karl S. and Hannemann K. 2012. Design and Optimization of a Small Scale M=8 Scramjet Propulsion System. In: *Space Propulsion 2012. Bordeaux: AAAF/ESA/CNES*.

[11] Langener T., Steelant J., Karl S. and Hannemann K. Layout. 2013. Design Verification of a Small Scale Scramjet Combustion Chamber. In: *ISABE 2013. Busan, Korea*, 1655.

[12] Babulin, A. A., Bosnyakov, S. M., Vlasenko, V. V., Engulatova, M. F., Matyash, S. V., and Mikhailov, S. V. 2016. Experience of validation and tuning of turbulence models as applied to the problem of boundary layer separation on a finite-width wedge. *Computational Mathematics and Mathematical Physics*, Vol. 56, No.6: 1020-1033.

[13] Vlasenko, V. V., and Shiryaeva, A. A. 2015. Computations of flow in a model high-speed combustor using different kinetic schemes. *Combustion and Explosion*, Vol.8, No.1: 116-125. (In Russian. ISSN: 2305-9117)

[14] Neyland, V., Bosniakov, S., Glazkov, S, Ivanov, A, Matyash, S, Mikhailov, S and Vlasenko, V. 2001. Conception of electronic wind tunnel and first results of its implementation. *Progress in Aerospace Sciences*, Vol. 37, 2001: 121-145.

[15] Bosnyakov, S, Kursakov, I, Lysenkov, A, Matyash, S, Mikhailov, S and Vlasenko, V. 2008. Computational tools for supporting the testing of civil aircraft configurations in wind tunnels. *Progress in Aerospace Sciences*, Vol. 44: 67–120.

[16] Vlasenko, V. V. and Sabelnikov, V. A. 1995. Numerical simulation of inviscid flows with hydrogen combustion behind shock waves and in detonation waves. *Combustion, Explosion and Shock Waves*, Vol.31, No.3: 376-389.

[17] Zeldovich, Y. V., & Zisin, U. A. (1941). On the theory of thermal stress. Flow in an exothermic stirred reactor, I. J. Tech. Phys, 11(6), 493-500.

[18] Cohen, D. S. (1971). Multiple stable solutions of nonlinear boundary value problems arising in chemical reactor theory. SIAM Journal on Applied Mathematics, 20(1), 1-13.